COMPARISON BETWEEN UNITARY ESPRIT AND SAGE FOR 3-D CHANNEL SOUNDING

Martin Tschudin,[1] *Christopher Brunner,*[2, 3] *Tobias Kurpjuhn,*[2] *Martin Haardt,*[3] *and Josef A. Nossek* [2]

1. Communication Technology Laboratory
Swiss Federal Institute of Technology, ETH-Zentrum
CH-8092 Zürich, Phone / Fax: +41 (1) 632-7639 / -1209
E-Mail: tschudin@nari.ee.ethz.ch

2. Institute for Circuit Theory and Signal Processing
Munich University of Technology, D-80290 Munich
Phone / Fax: +49 (89) 289-28511 / -28504
E-Mail: Christopher.Brunner@ei.tum.de

3. Siemens AG, ICN CA CTO 71
Hofmannstr. 51, D-81359 Munich
Phone / Fax: +49 (89) 722-29480 / -44958
E-Mail: Martin.Haardt@icn.siemens.de

Abstract – The detailed knowledge of the directional characteristics of the mobile radio channel is required to develop directional channel models and to design efficient smart antenna concepts for future mobile radio systems. In this paper, we examine the applicability and performance of two popular high-resolution parameter estimation schemes for directional channel sounding, namely subspace-based Unitary ESPRIT and the maximum-likelihood-based SAGE algorithm. To this end, an investigation of the resolution capability using a synthetic scenario is carried out for both schemes by means of Monte-Carlo simulations. The performance is also compared to the Cramér-Rao lower bound (CRLB). Moreover, we apply both parameter estimation schemes to propagation data generated by a ray-tracing model. This model is based on indoor channel measurements generated by the wideband channel sounding system *ECHO 24*. The channel measurements were taken inside a radio frequency shielded room (RFSR), an environment dominated by severe specular multipath and, therefore, can be considered a worst case scenario.

I. INTRODUCTION

Spatio-temporal radio channel measurements that include the dominant directions of arrival (DOAs), the corresponding propagation delays, and the complex amplitudes are desired in a variety of applications like sonar, radar, and cellular communications. In cellular communications, the channel estimates are required to design efficient smart antenna systems which exploit the inherent spatial diversity of the radio channel to achieve a significant increase in spectral efficiency.

Both parameter estimation schemes have been successfully applied to channel measurement data. In [12], the SAGE algorithm [3] is able to accurately estimate the dominant wavefronts in terms of their azimuth, delay, Doppler shift, and complex amplitude. The channel measurements were taken in downtown Aalborg, Denmark. In [15], the DOAs (azimuth and elevation), the delays, and the complex amplitudes of the dominant wavefronts of an indoor channel are estimated with the SAGE algorithm, while the same scheme was used to estimate the delays and azimuths of wavefronts in a picocellular environment [4]. A 2-D channel sounder [11] which is based on 2-D Unitary ESPRIT [7] and which provides paired azimuth and propagation delay estimates of the dominant multipath components has already been employed successfully in several field experiments conducted by Deutsche Telekom. In [6], the authors describe wideband direction-selective downlink sounding results. In several field experiments conducted by France Telecom in Paris, France, this algorithm has been employed successfully, too. Here, high-resolution estimates of the 2-D directions of arrival (azimuth and elevation) of the dominant propagation paths were determined with 2-D Unitary ESPRIT for each estimated impulse response tap delay separately.

In contrast to outdoor propagation [12], the slow motion of receiver and transmitter as well as scattering objects allows to neglect the Doppler effects in indoor environments. In the sequel, we will, therefore, characterize the dominant wavefronts in terms of their two-dimensional arrival angles (azimuth and elevation), their corresponding propagation delays, and their complex amplitudes. Channel sounding schemes which estimate these parameters are explained in [8] and [15] and are based on 3-D Unitary ESPRIT [7] and the SAGE algorithm [3, 15], respectively.

To circumvent the costs of development and implementation of new hardware for vector channel sounding, measurement concepts based on conventional single channel measurement techniques have been developed. The Rx antenna of the *ECHO 24* (**E**TH **C**hannel **S**ounder **O**perating at **24** GHz), for instance, can be moved along the 3-D coordinates of a virtual antenna array with the aid of a stepping motor driven positioning device [1]. The *ECHO 24* [14] uses a novel optical millimeter microwave generation principle in order to measure the complex impulse response of the channel with a bandwidth of 1 GHz. In a postprocessing step, high-resolution parameter estimation schemes such as 3-D Unitary ESPRIT and the SAGE algorithm are applied to these channel measurements.

[1] Note that virtual channel sounding allows a more flexible choice of antenna geometries such as, for example, a uniform cube array. On the other hand, the technique of virtual channel sounding can only be applied to time-invariant channels.

0-7803-5565-2/99/$10.00 © 1999 IEEE

Authorized licensed use limited to: T U MUENCHEN. Downloaded on October 15, 2008 at 05:34 from IEEE Xplore. Restrictions apply.

II. SIGNAL MODEL FOR 3-D CHANNEL SOUNDING

Space-Time Signal Model

In order to measure the channel of interest, a sounding signal is emitted which equals

$$u_c(t) = \Re\{u(t)\exp(2\pi f_0 t)\} \tag{1}$$

$$u(t) = \sum_{i=-\infty}^{\infty} a(t - iT), \tag{2}$$

where $a(t) = \sum_{n=0}^{N_c-1} a_n p(t - nT_c)$ is the pseudo-noise (PN) code with a_n denoting the (possibly complex) code chips, $p(t)$ is the shaping pulse, and the chips are of duration T_c. If a maximum length PN code is employed, the autocorrelation function (ACF) reads

$$r_{aa}(m) \triangleq \sum_{n=0}^{N_c-1} a_{(n+m)\mathrm{mod}N_c} a_n^* = \begin{cases} N_c & \text{if } m = \ell N_c, \\ & \ell \in Z \\ -1 & \text{otherwise} \end{cases}, \tag{3}$$

where a^* denotes complex conjugation. It is assumed that a finite number L of specular plane waves is impinging at the Rx location of the channel sounder. The Rx antenna is moved along the M sensors of a virtual antenna array located at $r_1, \ldots, r_M \in \mathbb{R}^3$ with respect to an arbitrary reference point with the aid of a motor driven positioning device for the three dimensions. At the m-th position of the virtual antenna array $y_{m,c}(t) = \Re\{y_m(t)\exp(2\pi f_0 t)\}$ is received by the Rx antenna. The narrowband assumption is valid since $B\frac{a}{c_0} \ll 1$ holds, where B marks the signal bandwidth, a denotes the size of the antenna array, and c_0 is the speed of light. Due to multipath propagation, L narrowband planar wavefronts of wavelength λ, azimuth ϕ_ℓ, elevation ϑ_ℓ, and complex amplitude α_ℓ, $1 \le \ell \le L$, are impinging on the virtual array. Thus, the noise-corrupted received signal vector at the output of the virtual antenna array can be written as the superposition

$$\begin{aligned} Y(t) &= \sum_{\ell=1}^{L} \overbrace{\alpha_\ell\, c_\ell\, u(t-\tau_\ell)}^{\triangleq s(t;\theta_\ell)} + N(t) && (4) \\ &= C_{2\mathrm{D}}\, \mathcal{A} \begin{bmatrix} u(t-\tau_1) \\ \vdots \\ u(t-\tau_L) \end{bmatrix} + N(t), && (5) \end{aligned}$$

where the 2-D array steering matrix

$$C_{2\mathrm{D}} \triangleq [\ c_1 \quad c_2 \quad \cdots \quad c_L\ ] \tag{6}$$

contains the 2-D directional information and $\mathcal{A} = \mathrm{diag}\{\alpha_\ell\}_{\ell=1}^{L}$, while $\theta_\ell \triangleq [\tau_\ell, \phi_\ell, \vartheta_\ell, \alpha_\ell]$ is the vector denoting the parameters of the ℓ-th wave. Two possibilities exist to characterize the 2-D directional information: If the incidence azimuth ϕ and the incidence elevation ϑ are used to describe the impinging waves, then

$$c_\ell \triangleq c(\phi_\ell, \vartheta_\ell) = [c_1(\phi_1, \vartheta_1), \ldots, c_M(\phi_L, \vartheta_L)]^{\mathrm{T}} \tag{7}$$

denotes the steering vector for the azimuth and elevation of the ℓ-th wave, whose components are given by $c_m(\phi, \vartheta) \triangleq \exp \jmath 2\pi\lambda^{-1} \langle e(\phi, \vartheta), r_m \rangle$ with $e(\phi, \vartheta) \triangleq [\cos(\vartheta)\cos(\phi), \cos(\vartheta)\sin(\phi), \sin(\vartheta)]^{\mathrm{T}}$ denoting the unit vector in $\mathbb{R}^3$ pointing toward the direction determined by ϕ, ϑ, respectively. Alternatively, the steering vector c can also be expressed as a function of the spatial frequencies $\mu^{(1)} \triangleq \pi\cos(\vartheta)\cos(\phi)$, $\mu^{(2)} \triangleq \pi\cos(\vartheta)\sin(\phi)$ resulting in

$$\begin{aligned} c_\ell &\triangleq c(\mu_\ell^{(1)}, \mu_\ell^{(2)}) \\ &= \left[c_1(\mu_\ell^{(1)}, \mu_\ell^{(2)}), \ldots, c_M(\mu_\ell^{(1)}, \mu_\ell^{(2)})\right]^{\mathrm{T}}. \end{aligned} \tag{8}$$

The vector $N(t) \triangleq [N_1(t), \ldots, N_M(t)]^{\mathrm{T}}$ denotes a M-D vector valued Gaussian noise process, whose first and second moments are given by

$$\begin{aligned} \mathbf{E}[N(t)] &= 0 \\ \mathbf{E}\left[N(t+\tau)N(t)^{\mathrm{H}}\right] &= N_0\, I_M\, \delta(\tau) \\ \mathbf{E}\left[N(t+\tau)N(t)^{\mathrm{T}}\right] &= 0. \end{aligned} \tag{9}$$

To avoid aliasing, all signals inside the sounder are bandlimited to $f_g = 1/2T_s$ prior to sampling at the rate $1/T_s = M_c/T_c$, where M_c denotes the number of samples per chip.

Space-Frequency Signal Model

For simplicity, we assume that a uniform rectangular array (URA) of omnidirectional sensors is located at the receiver. Assume that the URA contains M_1 sensors in x-direction and M_2 sensors in y-direction such that the noise-corrupted array measurements at time t are contained in the matrix $\mathcal{Y}_{2\mathrm{D}}(t)$, which is of size $M_1 \times M_2$. Hence, the noise-corrupted measurements equal $Y(t) = \mathrm{vec}\{\mathcal{Y}_{2\mathrm{D}}(t)\}$. Note that the 2-D array steering vectors of a URA may be written as Kronecker products of 1-D Vandermonde vectors, $c(\mu_i^{(1)}, \mu_i^{(2)}) = c(\mu_i^{(2)}) \otimes c(\mu_i^{(1)})$, where

$$c(\mu_i^{(r)}) = \left[\ 1 \quad e^{\jmath\mu_i^{(r)}} \quad \ldots \quad e^{\jmath(M_r-1)\mu_i^{(r)}}\ \right]^T,\ r = 1, 2. \tag{10}$$

Generation of Temporal Invariance Structure

Let $r_{pp}(\tau) = \mathrm{E}\{p(t+\tau)p^*(t)\}$ be the autocorrelation function of the chip waveform $p(t)$ such that ACF of the periodic sounding signal $u(t)$ with the correlator sequence $a(t) = \sum_{m=0}^{N_c-1} a_m p(t - mT_c)$ is a periodic repetition of $r_{pp}(\tau)$ with period $T = N_c T_c$ according to

$$r_{ua}(\tau) = \mathrm{E}\{u(t+\tau)a^*(t)\} = \sum_{n=-\infty}^{\infty} r_{aa}(n)\, r_{pp}(\tau - nT). \tag{11}$$

Authorized licensed use limited to: T U MUENCHEN. Downloaded on October 15, 2008 at 05:34 from IEEE Xplore. Restrictions apply.

Its Fourier series will be denoted as

$$R_{ua}(n) = \frac{1}{T}\int_{-T/2}^{T/2} r_{ua}(\tau)e^{-j2\pi n\frac{\tau}{T}}d\tau.$$

Then it is well known that the Fourier series of $r_{ua}(\tau-\tau_\ell)$ is given by $e^{-j2\pi n\frac{\tau_\ell}{T}}R_{ua}(n) = e^{jn\mu_\ell^{(3)}}R_{ua}(n)$, where $\mu_\ell^{(3)} = -2\pi\tau_\ell/T$ and the propagation delay $0 \le \tau_\ell < T$. If $r_{ua}(\tau)$ and $r_{ua}(\tau-\tau_\ell)$ are sampled above Nyquist rate, this property still holds for the DFTs of the resulting sequences. Due to the fact that the array measurements $Y(t) = y(t)$ are sampled at the rate $f_s = \frac{M_c}{T_c}$, the correlator (11) can also be realized in the discrete time domain. Using N_cM_c samples of the correlator output, we perform an (N_cM_c)-point DFT for each antenna. Note that only the spectral lines that correspond to the M_3 largest values of $R_{ua}(n)$ are computed. Thereby, the influence of the additive noise and the computational complexity can be reduced significantly. Note that the received signal after the correlator reads $y_{\text{cor}}(n) = \mathrm{E}\{y(t+nT_s)a^*(t)\}$. Let each row of $\mathcal{Y}_{\text{cor}} = [y_{\text{cor}}(1)\cdots y_{\text{cor}}(N_cM_c)]^T \in \mathbb{C}^{(M_1M_2)\times(N_cM_c)}$ contain N_cM_c samples of the output of the corresponding antenna after the correlator. Then the transformation of the space-time channel model to a space-frequency channel model is achieved by post-multiplying $\mathcal{Y}_{\text{cor}}$ by the $(N_cM_c)\times M_3$ DFT matrix W such that $\mathcal{Y}_{\text{3D}} = \mathcal{Y}_{\text{cor}}W$. It is well known that each column of W is of the form

$$w_\ell = \begin{bmatrix} 1 & e^{-j\ell\omega_0} & e^{-j2\ell\omega_0} & \dots & e^{-j(M_cN_c-1)\ell\omega_0} \end{bmatrix}^T,$$

where $\omega_0 = 2\pi/T$. Here, the columns of W compute $M_3 \le (N_cM_c)$ spectral lines centered at DC according to

$$W = \begin{bmatrix} w_{N_cM_c-(M_3-1)/2} & \cdots & w_0 & \cdots & w_{(M_3-1)/2} \end{bmatrix},$$

where we have invoked the wrap-around property of the DFT matrix. Due to the described Fourier properties and assuming that the channel is time-invariant over N snapshots, $\mathcal{Y}_{\text{3D}}(n)$ can be expressed as

$$\mathcal{Y}_{\text{3D}}(n) = \sum_{\ell=1}^{L}\alpha_\ell\cdot c(\mu_\ell^{(1)},\mu_\ell^{(2)})\,c(\mu_\ell^{(3)})^T\Lambda + \mathcal{N}(n), \quad (12)$$

where $\mathcal{N}(n)$ contains the additive noise in the space-frequency domain, the Vandermonde vector $c(\mu_\ell^{(3)})$ is defined in (10), and

$$\Lambda = \operatorname{diag}\{R_{uc}(n)\}_{n=N_cM_c-(M_3-1)/2}^{(M_3-1)/2}.$$

Apart from this diagonal matrix Λ, $\mathcal{Y}_{\text{3D}}(n)$ may be interpreted as a single snapshot of a (virtual) uniform cube array of the size $M_1\times M_2\times M_3$ corresponding to the nth repetition of the spreading sequence,

$$\begin{aligned} Y_{\text{3D}}(n) &= \operatorname{vec}\left\{\mathcal{Y}(n)\Lambda^{-1}\right\} \\ &= \sum_{\ell=1}^{L}\alpha_\ell\cdot c(\mu_\ell^{(3)})\otimes c(\mu_\ell^{(2)})\otimes c(\mu_\ell^{(1)}) + \operatorname{vec}\{\mathcal{N}(n)\}. \end{aligned}$$

Then the data matrix $Y_{\text{3D}} \in \mathbb{C}^{(M_1M_2M_3)\times N}$ equals

$$Y_{\text{3D}} = \begin{bmatrix} \operatorname{vec}\{\mathcal{Y}_{\text{3D}}(1)\Lambda^{-1}\} & \cdots & \operatorname{vec}\{\mathcal{Y}_{\text{3D}}(N)\Lambda^{-1}\} \end{bmatrix}.$$

If we assume ergodicity, the space-frequency covariance matrix may be estimated as[2] $R_{yy} = \frac{1}{N}\cdot Y_{\text{3D}}Y_{\text{3D}}^H$. Moreover, the corresponding noise covariance matrix

$$R_{nn} = \mathrm{E}\left\{\operatorname{vec}\{\mathcal{N}(n)\Lambda^{-1}\}\operatorname{vec}\{\mathcal{N}(n)\Lambda^{-1}\}^H\right\} \quad (13)$$

can be obtained in a similar fashion [1].

III. 3-D SAGE

Maximum-Likelihood Estimation of Superimposed Signals

The problem at hand is the ML-estimation of the parameter vectors θ_ℓ, $\ell = 1\dots,L$. We can apply the ML-estimator both to the space-time (4) and the space-frequency model (12), but we restrict our attention to the space-time case. Note that the parameter L is fixed to a value large enough to capture all the dominant impinging waves. The loglikelihood function of $\theta \triangleq [\theta_1,\dots,\theta_L]$ given an observation $Y(t) = y(t)$ over the time interval $[0,T)$ is [13]

$$\Lambda(\theta;y) \triangleq \frac{1}{N_0}\left[2\int_0^T \Re\left\{s^{\text{H}}(t';\theta)y(t')\right\}\mathrm{d}t' - \int_0^T \|s(t';\theta)\|^2\,\mathrm{d}t'\right], \quad (14)$$

where $s(t;\theta) \triangleq \sum_{\ell=1}^{L} s(t;\theta_\ell)$. The maximum-likelihood estimate (MLE) of θ is a value of θ that maximizes the function $\theta \mapsto \Lambda(\theta;y)$:

$$\hat\theta_{\text{ML}}(y) \in \arg\max_\theta\{\Lambda(\theta;y)\}. \quad (15)$$

The calculation of $\hat\theta_{\text{ML}}(y)$ is computationally prohibitive due to the high dimension of θ for large L and because no closed formula exists which expresses the global maxima of the nonlinear function $\theta \mapsto \Lambda(\theta;y)$. Since the values of the complex amplitudes maximizing $\Lambda(\theta;y)$ can be expressed in closed form as a function of the other parameters [5], the computation of the MLE of θ is a $3L$-D non-linear optimization procedure.

The SAGE Algorithm

The SAGE algorithm is a sequential way of finding the MLE (15) and has been derived in its general form in [3]. The method can be viewed as an extension of the EM algorithm [2] and is known for his faster convergence. The derivation of the SAGE algorithm for joint delay-azimuth-elevation estimation follows the rationale in [5]. In the following we sketch the basic ideas and the resulting formulas.

The $4L$-D parameter space is split up (subdivided) into $3L$ overlapping 2-D parameter subsets $\{\tau_\ell,\alpha_\ell\}$, $\{\phi_\ell,\alpha_\ell\}$, and

[2] Instead of this rectangular window, we may also use a sliding window to compute $\boldsymbol{R}_{yy}$.

Authorized licensed use limited to: T U MUENCHEN. Downloaded on October 15, 2008 at 05:34 from IEEE Xplore. Restrictions apply.

$\{\vartheta_\ell, \alpha_\ell\}$, where $\ell = 1 \ldots L$. The loglikelihood function (14) is then maximized with respect to the parameters of each subset while keeping the other parameters fixed. Since the MLE of α_ℓ can be derived in a closed form as a function of $[\tau_\ell, \phi_\ell, \vartheta_\ell]$, the $3L$ 2-D optimization problems further reduce to $3L$ 1-D optimizations. Analogous to [5], the coordinate-wise updating procedures to obtain the estimate $\hat{\theta}''$ for the parameters of wave ℓ given the estimate $\hat{\theta}'$, that contains all the previous estimates of the waves' parameters, is given as

$$\begin{aligned}
\hat{\tau}''_\ell &= \arg\max_{\tau} \left\{ \left| z\left(\tau, \hat{\phi}'_\ell, \hat{\vartheta}'_\ell;\ \hat{x}_\ell(t;\hat{\theta}')\right) \right| \right\}, \\
\hat{\phi}''_\ell &= \arg\max_{\phi} \left\{ \left| z\left(\hat{\tau}''_\ell, \phi, \hat{\vartheta}'_\ell;\ \hat{x}_\ell(t;\hat{\theta}')\right) \right| \right\}, \\
\hat{\vartheta}''_\ell &= \arg\max_{\vartheta} \left\{ \left| z\left(\hat{\tau}''_\ell, \hat{\phi}''_\ell, \vartheta;\ \hat{x}_\ell(t;\hat{\theta}')\right) \right| \right\}, \\
\hat{\alpha}''_\ell &= \tfrac{1}{MTP_u} z\left(\hat{\tau}''_\ell, \hat{\phi}''_\ell, \hat{\vartheta}''_\ell; \hat{x}_\ell(t;\hat{\theta}')\right),
\end{aligned} \tag{16}$$

where

$$z\left(\tau, \phi, \vartheta; \hat{x}_\ell(t;\hat{\theta}')\right) \triangleq c^{\mathrm{H}}(\phi, \vartheta) \int_0^T u^*(t'-\tau)\hat{x}_\ell(t';\hat{\theta}')\,\mathrm{d}t', \tag{17}$$

and

$$\begin{aligned}
P_u &\triangleq \frac{1}{T}\int_0^T |u(t)|^2 \mathrm{d}t, \\
\hat{x}_\ell\left(t;\hat{\theta}'\right) &\triangleq y(t) - \sum_{\ell'=1, \ell'\neq\ell}^{L} s\left(t;\hat{\theta}'_{\ell'}\right).
\end{aligned} \tag{18}$$

Carrying out once the above updating procedure for all L waves defines one iteration cycle of the SAGE algorithm. In (17) a twice-fold correlation is performed. At first $\hat{x}_\ell(t;\hat{\theta}')$, an estimate of a noise corrupted version of $s(t;\theta_\ell)$, is correlated with the transmitted signal $u(t)$. In a second step a spatial correlation is accomplished by the multiplication with $c^{\mathrm{H}}(\phi, \vartheta)$. The spatial correlation can be viewed as a 2-D beamforming scheme. Furthermore, the total energy $M\,T\,P_u$ collected over all sensors appears in (16) at the computation of $\hat{\alpha}''_\ell$ as a normalization factor. It is important to note that the 3-D SAGE algorithm implies no restrictions on the usable array geometries.

Initialization of the SAGE

An initialization method based on a successive cancellation scheme is proposed. Starting with the pre-initial setting $\hat{\theta}' = [0, \ldots, 0]$, for each $\ell = 1 \ldots L$,

$$\hat{\tau}''_\ell = \arg\max_{\tau} \left\{ \left| \int_0^T u^*(t'-\tau)\hat{x}_\ell(t';\hat{\theta}')\,\mathrm{d}t' \right|^2 \right\}, \tag{19}$$

$$(\hat{\phi}''_\ell, \hat{\vartheta}''_\ell) = \arg\max_{(\phi,\vartheta)} \left\{ \left| z\left(\hat{\tau}''_\ell, \phi, \vartheta; \hat{x}_\ell(t;\hat{\theta}')\right) \right| \right\}, \tag{20}$$

while the estimate of the complex amplitude is computed according to the last equation in (16). It should be noted that at the initialization of the ℓ-th wave all parameter estimates corresponding to $\ell' \geq \ell$ are still 0, i.e. $\hat{\theta}' = [\hat{\theta}'_1, \ldots, \hat{\theta}'_{\ell-1}, 0, \ldots, 0]$ and therefore the computation of (18) reduces to $\hat{x}_\ell(t;\hat{\theta}') = y(t) - \sum_{\ell'=1}^{\ell-1} s(t;\hat{\theta}'_{\ell'})$. Since in (19) ϕ' and ϑ' are unknown, $\hat{x}_\ell(t;\hat{\theta}')$ is incoherently summed over all sensors to provide the initial delay estimate. The 1-D beamformer for ϕ assuming $\vartheta_\ell = 0$ yields an erroneous estimate of the azimuth ϕ_ℓ if $\vartheta_\ell \neq 0$. Therefore, the initialization (20) is accomplished by a 2-D beamforming scheme.

IV. 3-D UNITARY ESPRIT

Two-dimensional centro-symmetric array geometries (such as a URA) are required by 3-D Unitary ESPRIT [7] to provide high-resolution estimates of the L three-dimensional frequency triplets $\mu_\ell^{(1)}$, $\mu_\ell^{(2)}$, and $\mu_\ell^{(3)}$ in a simple and efficient way. If desired, 3-D space-frequency smoothing (using subarrays of size $M_{\mathrm{sub}_1} \times M_{\mathrm{sub}_2} \times M_{\mathrm{sub}_3}$) can be applied to $Y_{3\mathrm{D}}$ as explained in [9].

In the first step of Unitary ESPRIT[3], forward-backward averaging is achieved by transforming the covariance matrices R_{yy} and R_{nn} to real matrices according to

$$G_{yy} = \mathrm{Re}\left\{Q_M^H R_{yy} Q_M\right\} \text{ and } G_{nn} = \mathrm{Re}\left\{Q_M^H R_{nn} Q_M\right\},$$

where Q_M denotes a left Π-real matrix that is also unitary. Then a basis of the estimated signal subspace E_s is determined through a real-valued generalized eigendecomposition

$$G_{yy}E_s = G_{nn}E_s \cdot \Sigma \quad \text{with} \quad \Sigma = \mathrm{diag}\left\{\sigma_i\right\}_{i=1}^{M}, \tag{21}$$

where the L dominant generalized eigenvectors of the matrix pair G_{yy} and G_{nn} form the columns of E_s. Using the real-valued signal subspace estimate E_s, three real-valued invariance equations are formed,

$$K_{(r)1}G_{nn}E_s\Upsilon_r \approx K_{(r)2}G_{nn}E_s \in \mathbb{R}^{m_r \times L}, \tag{22}$$

$r = 1, 2, 3$, where the three corresponding pairs of selection matrices $K_{(r)1}$ and $K_{(r)1}$ are constructed as described in [7, 9]. The three invariance equations (22) may be solved independently via least squares (LS), total least squares (TLS), or structured least squares (SLS) or jointly via a three-dimensional extension of SLS (3-D SLS), yielding three real-valued matrices $\Upsilon_r \in \mathbb{R}^{L\times L}$, $r = 1, 2, 3$. We use a Jacobi-type method to calculate a simultaneous Schur decomposition of several matrices. The Jacobi type method calculates the orthogonal matrix Θ such that the $R = 3$ matrices

$$U_r = \Theta^T \Upsilon_r \Theta, \quad 1 \leq r \leq R,$$

are approximately upper triangular in a least squares sense. The diagonal elements of U_r are denoted as $u_{\ell\ell}^{(r)}$, $1 \leq \ell \leq L$. Then automatically paired frequency estimates are obtained as

$$\mu_\ell^{(r)} = 2\arctan\left(u_{\ell\ell}^{(r)}\right), \quad 1 \leq \ell \leq L, \quad 1 \leq r \leq R.$$

[3] In the sequel, 3-D Unitary ESPRIT as presented in [7, 9] is modified slightly to take into account a noise correlation matrix R_{nn} that is not necessarily equal to the scaled identity matrix, i.e., colored noise.

Authorized licensed use limited to: T U MUENCHEN. Downloaded on October 15, 2008 at 05:34 from IEEE Xplore. Restrictions apply.

Further details with respect to 3-D Unitary ESPRIT are found in [7, 9]. The complex amplitudes can be estimated in the space-time domain as described in [8].

V. COMPARISON BASED ON SYNTHETIC SCENARIOS

In Monte-Carlo simulations, we have used a length 15 PN sequence with a bandlimited rectangular waveform of duration T_c. A URA of size 5×5 with interelement distance 0.45λ was employed. Two wavefronts ($\phi_1 = 90° + \Delta\phi/2$, $\vartheta_1 = 30° + \Delta\vartheta/2$, $\tau_1 = T_c$, $\alpha_1 = \sqrt{SNR}$, $\phi_2 = 90° - \Delta\phi/2$, $\vartheta_1 = 30° - \Delta\vartheta/2$, $\tau_2 = \tau_1 = T_c$, $\alpha_2 = \jmath\sqrt{SNR}$) with equal power are impinging on the array. The separation $\Delta\phi$ and $\Delta\vartheta$ of the two waves in the azimuth and elevation domain is expressed as multiples of the corresponding main lobe beam width $\phi_B = 29.404°$ and $\vartheta_B = 50.929°$. In accordance with the channel sounder *ECHO 24* [14], only one sequence is evaluated which corresponds to one snapshot in the space-frequency domain. Moreover, space-frequency smoothing using subarrays of size $M_{\text{sub}_1} = M_{\text{sub}_2} = 4$, $M_{\text{sub}_3} = 5$ is employed. The root mean square error (RMSE) of the estimated wave parameters (100 simulation runs were employed for each point) is used to compare the resolution capability of 3-D Unitary ESPRIT with 3-D SAGE as a function of $\Delta\phi$ and $\Delta\vartheta$. The RMSE of the parameters estimated with 3-D Unitary ESPRIT is slighty above the CRLB, while 3-D SAGE coincides with the CRLB, cf. Figure 1. For $\Delta\phi$ and $\Delta\vartheta$ converging to 0, the convergence time of 3-D SAGE increases such that full convergence is still not achieved after 100 iteration cycles. In this situation, the RMSE of 3-D SAGE deviates slightly from the CRLB.

VI. COMPARISON BASED ON MEASUREMENTS

Favourable geometrical properties of the radio frequency shielded room (RFSR), cf. Figure 3, allow us to efficiently set up a ray-trace model [4]. Based on the geometry of the RFSR and ray-tracing, we computed wave parameters of the 50 strongest paths ($N_c = 127$ length PN sequence, URA of size 7×7). For Unitary ESPRIT, the subarray size in the frequency domain was set to $M_{\text{sub}_3} = 97$, a nearly optimal value to yield maximal delay resolution. The spatial subarray size was chosen to 5×5. Figure 2 shows the results that can be achieved using 3-D SAGE and 3-D Unitary ESPRIT. Both schemes were able to estimate all impinging wavefronts.

The performance in terms of accuracy, memory requirements, and computational complexity of both schemes depends on numerous parameters: 3-D Unitary ESPRIT has

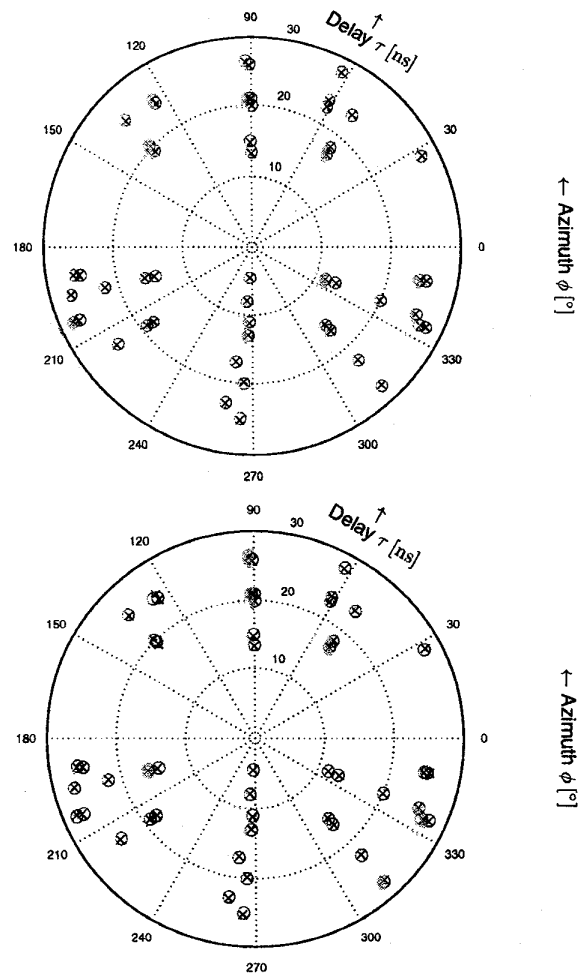

Figure 2: Delays and azimuths of the propagation scenario in the RFSR calculated with the virtual imaging method and estimated with SAGE (upper plot) and Unitary ESPRIT (lower plot).

been found to be sensitive to the size of the (temporal) subarray, M_{sub_3}, while the performance of 3-D SAGE is influenced by the choice of the angle and delay discretization which are used to compute the arguments of the maxima [5] in (16).

VII. CONCLUSIONS

It has been demonstrated that both 3-D Unitary ESPRIT and 3-D SAGE are high resolution schemes suitable to resolve the impinging waves at the measurement array with respect to their delay, incidence azimuth and incidence elevation in a severe multipath scenario.

[4] This ray-trace model has been verified with measurements [10] inside the RFSR taken with *ECHO 24* in combination with the 3-D SAGE algorithm. Note that *ECHO 24* uses a sequence length of $N_c = 1023$ and an oversampling factor of $M_c = 4$. To obtain a comparable delay resolution, 3-D Unitary ESPRIT requires an $M_{\text{sub}_3} > 300$, thereby causing high memory demands. The memory requirements may be reduced significantly if the channel delay spread (as in this case) is much smaller than the duration of the correlation sequence. This is under current investigation.

[5] Typically, the azimuth, elevation, and delay estimates are computed with finite quantization. If the improvement of the parameter estimate (16) from one iteration cycle to the other becomes smaller than this quanitization, the estimates saturate before complete convergence is achieved

Authorized licensed use limited to: T U MUENCHEN. Downloaded on October 15, 2008 at 05:34 from IEEE Xplore. Restrictions apply.

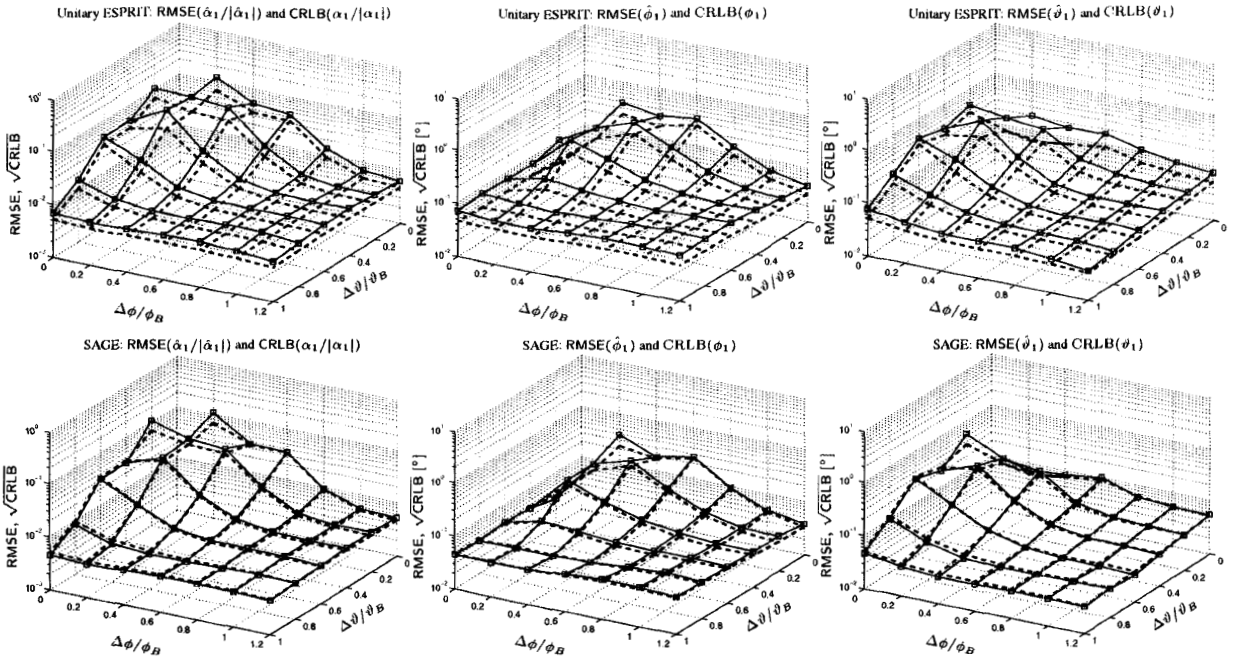

Figure 1: $\sqrt{\text{CRLB}}$ and simulated RMSE as a function of $[\Delta\phi, \Delta\vartheta]$; ▪ ▪ ▪ ▪ $\sqrt{\text{CRLB}}$, $\frac{\Delta\tau}{T_c} = 0$ □——□ RMSE, $\frac{\Delta\tau}{T_c} = 0$, SNR= $20dB$

REFERENCES

(1) C. Brunner, M. Haardt, and J. A. Nossek, "2-D rake receiver in the space-frequency domain for the uplink of WCDMA", in *Proc. 6th IEEE International Workshop on Intelligent Signal Processing and Communication Systems. (ISPACS '98)*, vol. 2, pp. 551–555, Melbourne, Australia, Nov. 1998.

(2) M. Feder and E. Weinstein, "Parameter estimation of superimposed signals using the EM algorithm", *IEEE Trans. Acoust., Speech, Signal Processing*, vol. ASSP-36, no. 4, pp. 477–489, Apr. 1988.

(3) J. A. Fessler and A. O. Hero, "Space-alternating generalized expectation-maximization algorithm", *IEEE Trans. Signal Processing*, vol. 42, pp. 2664–2677, Oct. 1994.

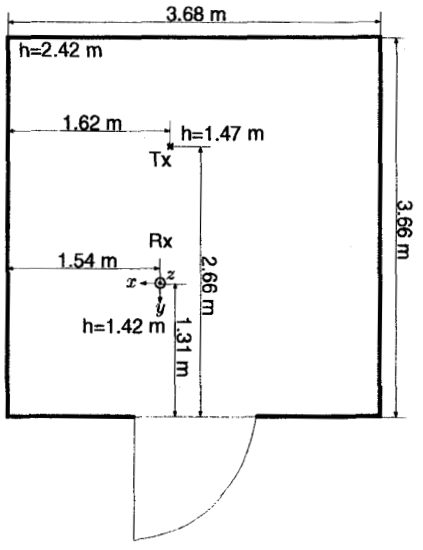

Figure 3: Sketch of the RFSR.

(4) B. Fleury, D. Dahlhaus, R. Heddergott, and M. Tschudin, "Wideband angle of arrival estimation using the sage algorithm", in *Proc. IEEE ISSSTA*, vol. 1, pp. 79–85, Mainz, September 1996.

(5) B. H. Fleury, M. Tschudin, R. Heddergott, D. Dahlhaus, and K. Pedersen, "Channel parameter estimation in mobile radio environments using the SAGE algorithm", *IEEE Journal Select. Areas Commun.: Wireless Communications Series*, vol. 17, Mar. 1999.

(6) J. Fuhl, J. P. Rossi, and E. Bonek, "High-resolution 3D direction-of-arrival determination for urban mobile radio", *IEEE Trans. Antennas and Propagation*, vol. 45, pp. 672–682, Apr. 1997.

(7) M. Haardt, *Efficient One-, Two-, and Multidimensional High-Resolution Array Signal Processing*, Ph. D. dissertation, Technical University of Munich, Institute of Network Theory and Circuit Design, Germany, 1996, Shaker Verlag, ISBN 3-8265-2220-6.

(8) M. Haardt, C. Brunner, and J. A. Nossek, "Efficient high-resolution 3-D channel sounding", in *Proc. 48th IEEE Vehicular Technology Conf. (VTC '98)*, pp. 164–168, Ottawa, Canada, May 1998.

(9) M. Haardt and J. A. Nossek, "Simultaneous Schur decomposition of several non-symmetric matrices to achieve automatic pairing in multidimensional harmonic retrieval problems", *IEEE Trans. Signal Processing*, vol. 46, pp. 161–169, Jan. 1998.

(10) R. Heddergott, P. Truffer, and M. Tschudin, "Comparison of high resolution channel parameter measurements with ray tracing simulations in a multipath environment", in *3rd European Mobile Radio Conference (EPMCC'99)*, pp. 1–6, Paris, France, Mar. 1999.

(11) U. Martin, "A directional radio channel model for densely build-up urban area", in *Proc. 2nd European Personal Mobile Communications Conference*, pp. 237–244, Bonn, Germany, Sept. 1997.

(12) K. I. Pedersen, B. H. Fleury, and P. E. Mogensen, "High resolution of electromagnetic waves in time-varying radio channels", in *Proc. 8th IEEE Int. Symp. on Personal, Indoor and Mobile Radio Commun. (PIMRC)*, Helsinki, Finland, Sept. 1997.

(13) H. V. Poor, *An Introduction to Signal Detection and Estimation*, Springer-Verlag, New York, NY, 1988.

(14) P. Truffer and R. Sibilia, "Wideband channel sounder with optica antenna feeding", Tech. Rep. COST 259 TD (97) 044, COST259, Lisbon, Portugal, Sept. 1997.

(15) M. Tschudin, R. Heddergott, and P. Truffer, "Validation of high resolution measurement technique for estimating the parameters fo impinging waves in indoor environments", in *Proc. 48th IEEE Personal Indoor and Mobile Radio Conf. (PIMRC '98)*, Boston, USA, Sept. 1998.

Authorized licensed use limited to: T U MUENCHEN. Downloaded on October 15, 2008 at 05:34 from IEEE Xplore. Restrictions apply.